Publication Year	2017
Acceptance in OA@INAF	2020-08-28T12:32:16Z
Title	The olivine-dominated composition of the Eureka family of Mars Trojan asteroids
Authors	Borisov, G.; Christou, A.; Bagnulo, S.; CELLINO, Alberto; Kwiatkowski, T.; et al.
DOI	10.1093/mnras/stw3075
Handle	http://hdl.handle.net/20.500.12386/26951
Journal	MONTHLY NOTICES OF THE ROYAL ASTRONOMICAL SOCIETY
Number	466

Monthly Notices
of the
ROYAL ASTRONOMICAL SOCIETY

MNRAS **466,** 489–495 (2017)
Advance Access publication 2016 November 29

doi:10.1093/mnras/stw3075

The olivine-dominated composition of the Eureka family of Mars Trojan asteroids

G. Borisov,[1,2★] A. Christou,[1★] S. Bagnulo,[1] A. Cellino,[3] T. Kwiatkowski[4] and A. Dell'Oro[5]

[1]*Armagh Observatory and Planetarium, College Hill, Armagh BT61 9DG, UK*
[2]*Institute of Astronomy and National Astronomical Observatory, 72, Tsarigradsko Chaussée Blvd., BG-1784 Sofia, Bulgaria*
[3]*INAF – Osservatorio Astrofisico di Torino, via Osservatorio 20, I-10025 Pino Torinese (TO), Italy*
[4]*Astronomical Observatory, Adam Mickiewicz University, ul. Słoneczna 36, PL-60-286 Poznań, Poland*
[5]*INAF – Osservatorio Astrofisico di Arcetri, Largo E. Fermi 5, I-50125 Firenze, Italy*

Accepted 2016 November 23. Received 2016 November 22; in original form 2016 October 18

ABSTRACT

We have used the XSHOOTER echelle spectrograph on the European Southern Obseratory (ESO) Very Large Telescope (VLT) to obtain UVB–VIS–NIR (ultraviolet–blue (UVB), visible (VIS) and near-infrared (NIR)) reflectance spectra of two members of the Eureka family of L5 Mars Trojans, in order to test a genetic relationship to Eureka. In addition to obtaining spectra, we also carried out *VRI* photometry of one of the VLT targets using the 2-m telescope at the Bulgarian National Astronomical Observatory – Rozhen and the two-channel focal reducer. We found that these asteroids belong to the olivine-dominated A, or S_a, taxonomic class. As Eureka itself is also an olivine-dominated asteroid, it is likely that *all* family asteroids share a common origin and composition. We discuss the significance of these results in terms of the origin of the martian Trojan population.

Key words: techniques: imaging spectroscopy – techniques: photometric – minor planets, asteroids: individual: Trojan asteroids – planets and satellites: individual: Mars.

1 INTRODUCTION

The so-called Mars Trojans are asteroids located in the L4 or L5 Lagrangian points of Mars. They are thought to have been there since the very early phases of the Solar system's history. There were nine confirmed Martian Trojans in total as of 2015, of which eight were at L5 and 1 at L4. Occupants of the Mars Trojan clouds might represent a small set of survivors of an early generation of planetesimals from which the inner Solar system was built. The long-term stability of the Mars Trojan clouds has been extensively investigated by Scholl, Marzari & Tricarico (2005). According to these authors, in the L4 and L5 regions of Mars, there are combinations of orbital eccentricity and inclination that are stable over time-scales comparable to the Solar system's age. Of the eight L5 Trojans, seven (including Eureka) form the Eureka family, whose existence has been pointed out by Christou (2013) and de la Fuente Marcos & de la Fuente Marcos (2013). Due to its compactness, this is probably a genetic family rather than a random grouping of orbits. It formed sometime in the last Gyr (Ćuk, Christou & Hamilton 2015). The members of the Eureka asteroid family are also stable Trojans. For this reason, the discovery that asteroid (5261) Eureka belongs to the rare A taxonomic class (Rivkin et al. 2007; Lim et al. 2011) is very interesting. The spectral reflectance properties of A-class asteroids have been interpreted as diagnostic of an overall composition rich in the mineral olivine [$(Mg^{++}, Al^{++})_2SiO_4$], a magnesium iron silicate that is a primary component of the Earth's mantle and – supposedly – of the other terrestrial planets. The low abundance of olivine-rich objects among asteroids is an old conundrum. In particular, the existence of metal meteorites suggests that during the early phases of the Solar system's history, several planetesimals reached sizes sufficient for complete thermal differentiation due to the heat produced by the decay of short-lived isotopes, primarily ^{26}Al. Metal meteorites are interpreted in this scenario as fragments of the metal-rich cores of such differentiated bodies, exposed after their complete collisional disruption. In this context, one should expect that olivine-rich meteorites and asteroids should be common because olivine is a primary component of the mantles of differentiated bodies. However, this prediction is not borne out of the observations. Asteroids belonging to the olivine-rich A class, or even to the fairly similar S_a subclass of the S taxonomic complex (Bus & Binzel 2002; DeMeo et al. 2009b), are quite rare. At the end of the 1990s, several authors proposed that the original olivine-rich asteroids were 'battered to bits' by collisions and had thus disappeared long ago (Burbine, Meibom & Binzel 1996; Chapman 1997). Whatever the cause of such disappearance, collisional evolution or, perhaps more likely,

★ E-mail: gbb@arm.ac.uk (GB); aac@arm.ac.uk (AC)

© 2016 The Authors
Published by Oxford University Press on behalf of the Royal Astronomical Society

Downloaded from https://academic.oup.com/mnras/article-abstract/466/1/489/2608775 by INAF Torino (Osservatorio Astrofisico di Torino) user on 14 July 2020

massive removal of the original planetesimals accreted in the main belt, as predicted by the Grand Tack and Nice models of early evolution of the Solar system (Walsh et al. 2011, 2012), only a small number of survivors belonging to the A class can be found among the current asteroid population. As a consequence, the discovery of an A-class asteroid confined in a special dynamical environment within the terrestrial planet region suggests that the other members of the Eureka family also deserve a careful investigation. Based on these considerations, we began an observing campaign to obtain information on the spectral reflectance properties of these objects. This is a challenging task because, in spite of their relative proximity to the Earth, Mars Trojans are faint. Their observation therefore requires the use of large-aperture instruments.

In our investigation, we used XSHOOTER, the first European Southern Observatory (ESO) second-generation instrument developed for the Very Large Telescope (VLT; Vernet et al. 2011), which is currently mounted on VLT Unit 2 Kueyen. XSHOOTER is a spectrograph capable of obtaining spectra from 300 to 2480 nm in a single shot at high spectral resolution (from 3000 up to 10 000). In the following sections, we present the spectra we obtained for two members of the Eureka family, and compare them with the available reflectance spectra for Eureka itself.

We also obtained some limited spectrophotometric information by carrying out multiband *VRI* photometry. We used the two-channel focal reducer – Rozhen (FoReRo2) of the 2 m Ritchey–Chrétien–Coudé telescope at the Bulgarian National Astronomical Observatory (BNAO) to obtain $(V - R)$ and $(V - I)$ colours of a member of the Eureka family, also one of our two targets observed with XSHOOTER. The colour indices were compared with the results obtained by Neese (2010), and with the average values of the colour indices for different asteroid taxonomic classes.

This paper is organized as follows. In Section 2, we present our VLT and Rozhen observations. The adopted procedures for data reduction are described in Section 3, and the results in Section 4, separately for spectroscopy and multiband photometry. Our main conclusions and a general discussion of our results is given in Section 5.

2 OBSERVATIONS

We used XSHOOTER during two nights, FoReRo2 during two nights as well and ACAM for one night. The objects that were observed are as follows: XSHOOTER: (385250) 2001 DH47, (311999) 2007 NS2 and spectral solar analogue star HD 67010; FoReRo2: (385250) 2001 DH47, (289) Nenetta [an asteroid with an olivine-dominated surface (Sanchez et al. 2014)] and Stetson standard field L101; ACAM: (3819) Robinson [an asteroid with an olivine-dominated surface (Sanchez et al. 2014)] and Stetson standard field L104. Details of our observations are presented in Tables 1–3.

2.1 Spectroscopy

2.1.1 XSHOOTER

This instrument is an echelle spectrograph with an almost fixed spectral setup. The observer can choose between SLIT (and slit width) and IFU (integral field unit) modes. Here we used the SLIT

Table 1. Observations – XSHOOTER@VLT.

Object	Date	UT	Airmass	Apparent magnitude	Spectral arm	Exposure time (s)
		03:04	1.174		UVB	3040
(385250) 2001 DH47	2016 February 2	|	|	19.00	VIS	3280
		04:07	1.377		NIR	3600
					UVB	40
HD 67010	2016 February 2	05:15	1.158	8.69	VIS	30
					NIR	100
		01:37	1.022		UVB	3040
(311999) 2007 NS2	2016 March 2	|	|	19.05	VIS	3280
		02:21	1.367		NIR	3600
					UVB	40
HD 67010	2016 March 2	03:30	1.168	8.69	VIS	30
					NIR	100

Table 2. Observations – FoReRo2@2mRCC.

Object	Date	UT	Airmass	Apparent magnitude	Filter	Exposure time (s)
	2016 February 6	22:00	1.30		*I*	10 × 300
(385250) 2001 DH47	|	|	|	18.55	*R*	10 × 300
	2016 February 7	01:00	1.50		*V*	10 × 300
		20:00	1.15		*I*	3 × 300
(289) Nenetta	2016 February 6	|	|	14.13	*R*	3 × 300
		21:00	1.25		*V*	3 × 300
		19:50	2.10	12.64	*V*	3 × (5 × 60)
Stetson L101	2016 February 6	21:30	1.50	|	*R*	3 × (5 × 60)
		23:00	1.30	20.64	*I*	3 × (5 × 60)

Downloaded from https://academic.oup.com/mnras/article-abstract/466/1/489/2608775 by INAF Torino (Osservatorio Astrofisico di Torino) user on 14 July 2020

Table 3. Observations – ACAM@WHT.

Object	Date	UT	Airmass	Apparent magnitude	Filter	Exposure time (s)
		06:10	1.94		g'	3×80
(3819) Robinson	2016 March 11	|	2.02	16.36	r'	3×60
		06:25	2.12		i'	3×60
		02:30	1.145	12.75	g'	(4×5) and (3×15)
Stetson L104	2016 March 11			|	r'	(4×5) and (3×10)
		06:00	1.853	21.12	i'	(4×5) and (3×15)

mode. A detailed description of the instrument is available at Vernet et al. (2011) and ESO's webpage.[1] This spectrograph has the ability to simultaneously obtain data over the entire 300–2480 nm spectral range by splitting the incoming light from the telescope into three beams, each sent to a different arm: ultraviolet–blue (UVB), visible (VIS) and near-infrared (NIR). Using two dichroic filters, the light is first sent to the UVB arm, then to the VIS arm and, finally, the remaining light arrives at the NIR arm. The disadvantage of this choice of optical light path is the high thermal background in the K-region of the NIR spectrum. The observations are presented in Table 1. Observations were done in nodding mode to facilitate subsequent sky signal estimation and subtraction.

2.2 *VRI* photometry

2.2.1 FoReRo2

The instrument is a two-channel focal reducer that adapts the imaging elements of the detector to the characteristic size of the object or the seeing disc. FoReRo2 was built mainly for observations of cometary plasma but has been proved suitable for many other tasks (Jockers et al. 2000). Behind the RC (Cassegrain) focus, the light beam is recollimated by a lens collimator. A dichroic mirror reflects the blue part of the spectrum and transmits the red part. For each channel, camera lenses form reduced images of the Cassegrain focal plane, which are recorded by two CCD systems. Filters are placed into the parallel beam after colour separation. For this investigation, we used *VRI* standard filters; therefore, only the red channel of the instrument was in operation. The observations are presented in Table 2.

2.2.2 ACAM

The ACAM instrument of the 4.2-m William Herschel Telescope (WHT) at the Observatorio del Roque de los Muchachos (La Palma, Spain) was used to obtain SDSS photometry of asteroid (3819) Robinson. The observations are presented in Table 3.

3 DATA REDUCTION

3.1 XSHOOTER

To reduce the XSHOOTER spectra, we first processed the data through the ESO ESOREFLEX pipeline version 2.6.8. All spectra were reduced under the assumption of point-like sources and had their instrument signature removed, i.e. de-biased, flat-fielded, wavelength-calibrated, order-merged, extracted, sky-subtracted and, finally, flux-calibrated.

[1] http://www.eso.org/sci/facilities/paranal/instruments/xshooter.html

To achieve a signal-to-noise ratio (S/N) sufficient for scientific analysis, the reduced 1D spectra for both the asteroid and solar analogue standard stars were then rebinned in 20 nm steps. Subsequently, the spectrum of the asteroid was divided by the solar analogue spectrum, the result normalized to unity at 550 nm and again smoothed using a floating average with different wavelength steps in the VIS and NIR regions.

Finally, we carried out running sigma clipping of the data with a 20 nm window in wavelength and a 3σ criterion. During this stage, we excluded sections of the spectra affected by high telluric line contamination in the following wavelength intervals: 0.90–1.00, 1.35–1.50 and 1.80–1.90 μm, as suggested by Moehler et al. (2014) and Gourgeot et al. (2015).

3.2 FoReRo2

All imaging data had their instrument signature removed as well by de-biasing and flat-fielding. The images in I were de-fringed using the median I image combined from all I images for the night. Standard DAOPHOT aperture photometry with aperture size 2× fullwidthathalf-maximum(FWHM) was performed. Aperture correction, which was measured through a large aperture using the growth-curve method (Stetson 1990), was applied in order to place the instrumental magnitudes of the observed point source objects, which were measured through a small aperture (2×FWHM), on the same system as those of the standard stars. Stetson standard field L101, observed on three different airmasses, was used for obtaining extinction coefficients in each filter. Linear regression fits for magnitude–magnitude and colour–colour calibration were performed as well. Then, the instrumental magnitudes of the asteroid targets were absolutely calibrated using coefficients from those fits, and, finally, their true $(V - R)$ and $(V - I)$ colours were computed.

3.3 ACAM

All imaging data had their instrument signature removed as well by de-biasing and flat-fielding. The same calibration procedure as the one for FoReRo2 was performed using Stetson standard field L104. The photometry performed in SDSS g' r' i' filters was converted into *VRI* using relations presented by Jordi, Grebel & Ammon (2006).

4 RESULTS

4.1 Spectroscopy

The resulting XSHOOTER spectra are represented by black lines in Figs 1–4.

In Figs 1 and 2, we show, apart from the reflectance spectra of our two targets, a spectrum of (5261) Eureka (blue) obtained on 2005 May 19 (Rayner et al. 2003, spectrum available online at

Downloaded from https://academic.oup.com/mnras/article-abstract/466/1/489/2608775 by INAF Torino (Osservatorio Astrofisico di Torino) user on 14 July 2020

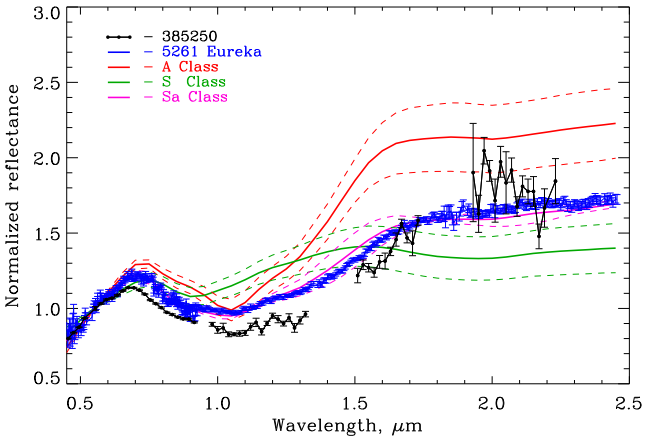

Figure 1. (Colour online) Reflectance spectrum of the asteroid (385250) 2001 DH47 (black dotted) compared with average spectra for A (red), S (green) and S_a (purple) taxonomic classes. The spectrum of (5261) Eureka is overplotted in blue.

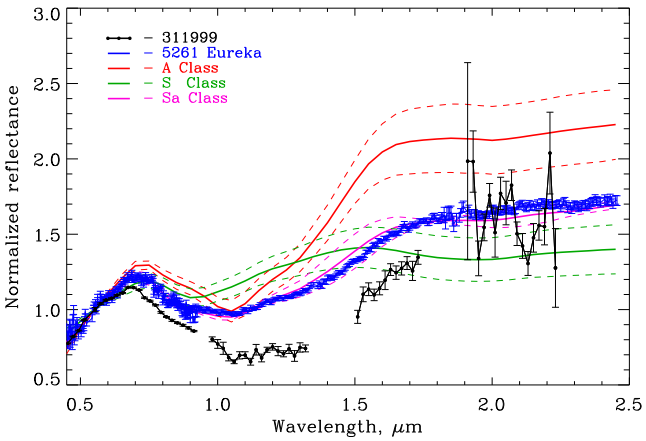

Figure 2. (Colour online) Reflectance spectrum of the asteroid (311999) 2007 NS2 (black dotted line) compared with average spectra for A (red), S (green) and S_a (purple) taxonomic classes. The spectrum of (5261) Eureka is overplotted in blue.

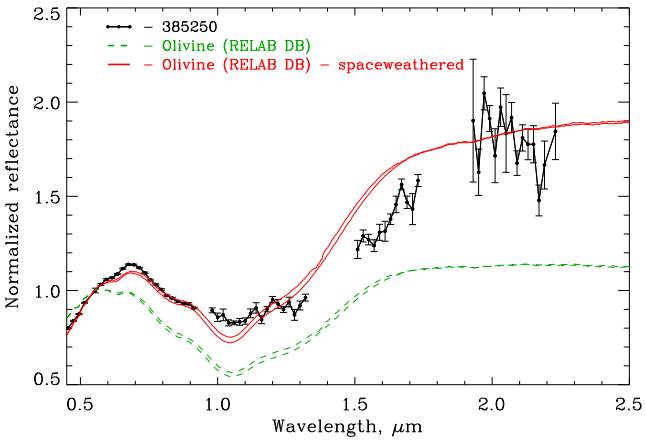

Figure 3. Reflectance spectrum of asteroid (385250) 2001 DH47 (black line with points) compared with two olivine spectra from RELAB (green dashed line) and the same spectra divided by a slope to simulate space weathering (red line).

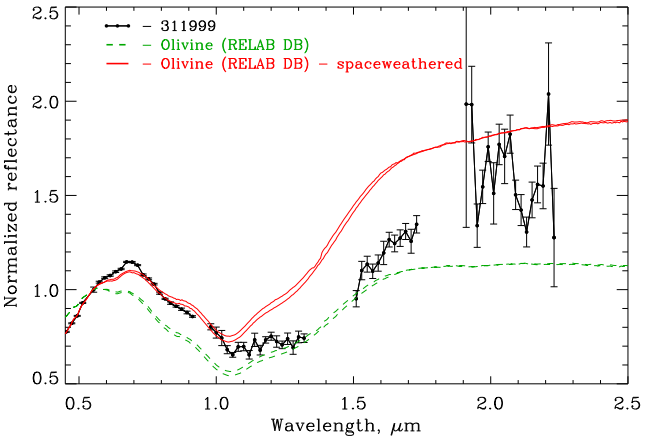

Figure 4. Reflectance spectrum of the asteroid (311999) 2007 NS2 (black line with points) compared with two olivine spectra from RELAB (green dashed line) and the same spectra divided by a slope to simulate space weathering (red line).

http://smass.mit.edu/minus.html - sp41) and average spectra for the A (red), S (green) and S_a (purple) classes in the DeMeo et al. (2009b) taxonomy produced from data available in the PDS data base (EAR-A-VARGBDET-5-BUSDEMEOTAX-V1.0; DeMeo et al. 2009a) as point-by-point means of 6, 144 and 2 asteroids, respectively. We find a 1 μm absorption feature for both Eureka family members where the reflectance minimum is located slightly longward of 1 μm. This is also the case for the A- and S_a-type spectra and a diagnostic feature of an olivine-rich surface.

The regions with high telluric lines contamination, excluded from our analysis (see Section 3), do not affect distinguishing between the S, A and S_a classes, as the 1 μm feature in S-class spectra is below 0.9 μm. We also note the higher and flatter reflectance of the S-class spectrum in the region of 1.0–1.5 μm, which distinguishes it from the other spectra.

Overall, the two asteroid spectra are in better agreement with an Sa than an A taxonomy, both in the visible and the infrared (IR). Eureka, also an Sa-type asteroid in the DeMeo et al. classification scheme,[2] appears to be somewhat more reflective than 311999 and 385250 from ∼0.6 up to at least 1.3 μm. Eureka's 1 μm feature is unique among A/S_a types. It is the only object with that particular band shape. The spectra of the two new objects, which we classify as S_a, though they have a lower S/N ratio, appear consistent with Eureka's. At 2 μm, the reflectivities of the three objects are indistinguishable from each other; although possibly a consequence of the lower S/N, we believe it to be a real feature of the spectrum.

Seeking to strengthen the case for the presence of olivine, we compared our spectra with a number of laboratory olivine spectra from the RELAB data base. Exposure of asteroid surfaces to the space environment changes their optical properties. Therefore, we applied a simple space weathering correction to the laboratory spectra prior to the comparison by dividing the olivine RELAB spectra with a first-order polynomial. Through visual inspection, we found that spectra MS-CMP-042-A and MS-CMP-014 (green lines in Figs 3 and 4 altered by our space-weathering correction, red lines) are reasonable matches to the asteroid spectra. The first laboratory spectrum corresponds to unprocessed pure olivine; the second, also of pure olivine,

[2] The observed coincidence between the Sa spectrum and that of Eureka is not accidental; this asteroid is one of only two objects whose spectra define this taxonomic class.

Downloaded from https://academic.oup.com/mnras/article-abstract/466/1/489/2608775 by INAF Torino (Osservatorio Astrofisico di Torino) user on 14 July 2020

is altered by laser irradiation to simulate micrometeoroid impacts. Although it is difficult to obtain a good match over the entire wavelength interval covered by our spectra, by restricting ourselves to the visible part, and the simple space-weathering model, we find that our best match (red lines) fits the visible part of our spectra quite well, particularly the minor absorption features around 0.63 and 0.8 μm. Progressing further along this line of investigation probably requires a more refined model of space-weathering effects, which is beyond the scope of this paper.

4.2 *VRI* photometry

Visible colour photometry can be used as a consistency check and also to eliminate candidate spectroscopic classes. Its advantage is that it is generally applicable to fainter objects than spectroscopy. On the other hand, unambiguous taxonomic classification and mineralogical interpretation typically requires detailed knowledge of the reflectance as a function of wavelength as well as extending observations into the IR. Our purpose here is to identify, through direct measurements, the domain that Eureka, its family members and asteroids of a similar mineralogical composition occupy in colour space with a view to possible future observations of the fainter Eureka family asteroids.

The $(V - R)$ and $(V - I)$ colour indices for one of the objects, (385250) 2001 DH47, were derived from three series of 10 exposures, acquired in the *I*, *R* and *V* filters with FoReRo2 at BNAO. As some images were of inferior quality, only eight exposures in each filter were used, from which average values were computed.

Because of the faintness of the asteroid target, we used relatively long exposures of 300 s. This resulted in a duty cycle of 318 s and extended the observing run to 3 h. On 2016 January 8, we carried out photometric observations of (385250) 2001 DH47. A rotation period of $P \approx 4.0 \pm 0.8$ h and a peak-to-peak amplitude of 0.6 mag were derived (Borisov, Christou & Unda-Sanzana 2016). The asteroid light variation could potentially introduce systematic effects in the colour indices.

We used those parameters to understand the effect of the asteroid light curves in determining the colour indices obtained from the Rozhen data. Due to the relatively high uncertainty in the rotation period *P* and a long time interval between the January 6 and February 8 observations, we could not determine accurate rotation phases for our exposures. In addition, the January 8 observations were performed at a solar phase angle of 30.°4, while on February 6, the phase angle was 8.°2. Assuming the classic amplitude—phase relationship with $m = 0.02$ mag deg^{-1} (Gutiérrez et al. 2006), we estimated the light-curve amplitude of (385250) 2001 DH47 on February 6 to be 0.4 mag.

A simulated light curve of (385250) 2001 DH47, with a simple sinusoidal shape, rotation period $P = 4$ h and peak-to-peak amplitude $A = 0.4$ mag, is presented in Fig. 5, with the relative times of the *I*, *R* and *V* exposures superimposed on the light curve. The rotation phase of the first point is arbitrary, but the intervals between consecutive points reflect the actual timings of the exposures. In this model, the average brightness in the *I*, *R* and *V* filters would be 0.084, −0.080 and 0.102, respectively, and the colour indices would be $(V - I) = 0.018$ mag, $(V - R) = 0.183$ mag. In reality, the rotation phase of the first point of the observing sequence is unknown, so we repeated the computations with phase shifts from 0.02 to 1 in steps of 0.025. Also, for each phase shift, we computed colour indices while changing the rotation period from 3.2 to 4.8 h, in steps of 0.1 h. In this way, we obtain $39 \times 17 = 663$ pairs of colour indices $(V - I)$ and $(V - R)$, which allowed us to estimate

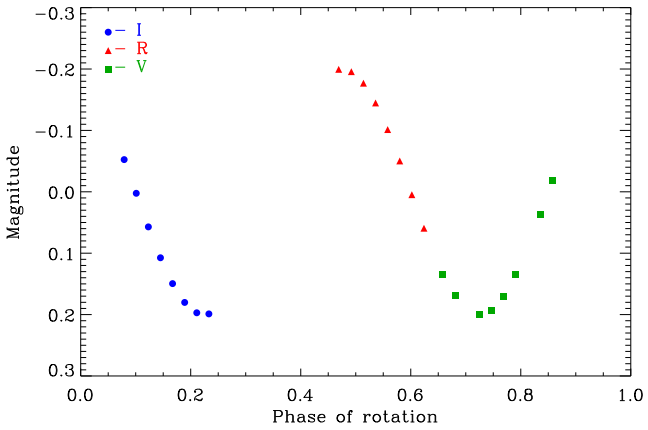

Figure 5. A simulated light curve of (385250) 2001 DH47 with an assumed sinusoidal brightness variation, rotation period of 4 h and a peak-to-peak amplitude of 0.4 mag. While the rotation phase of the first point is arbitrary, data intervals reflect actual times of the exposures in the *I*, *R* and *V* filters.

the systematic uncertainty of the colour indices computed from the Rozhen observations due to asteroid brightness variation.

To estimate the statistical uncertainties resulting from the random scatter of the measurements, we used formal sigma values given by the DAOPHOT package for each single *V*, *R*, *I* instrumental magnitude. These were then propagated to final estimates of the $(V - I)$ and $(V - R)$ colours, resulting in sigma values of 0.05 and 0.04 mag, respectively. The former is slightly greater than the latter due to the greater noise of the *I*-filter measurements.

Fig. 6 presents the $(V - R)$ and $(V - I)$ colour indices of (385250) 2001 DH47, compared with the average colours of all taxonomic classes in the Tholen (1984) classification scheme, as given in Dandy, Fitzsimmons & Collander-Brown (2003), as well as the S_a and S_r classes in the Bus & Binzel (2002) classification. The systematic uncertainty due to the light curve is shown as an ellipse. The random measurement uncertainties of the colour indices are represented by the error bars.

S_a and S_r classes in the Bus & Binzel (2002) taxonomy – distinct from the classes of the same name in the DeMeo et al. (2009b) taxonomy – are intermediate between S and A, and S and R, respectively. The visible (0.44–0.92 μm) spectra that define these classes have a very steep ultraviolet slope shortward of 0.7 μm. The 1 μm absorption feature, while deep and clearly visible in S_r, is shallow and not well defined in S_a, which shows that it might be shifted above 1 μm and can be associated with a presence of olivine. To compute colours representing the S_a and S_r classes, we searched for asteroids belonging to those classes in the SMASS II data base. SDSS colours for five S_a and three S_r objects included in the SDSS data base of moving objects (EAR-A-I0035-5-SDSSTAX-V1.1; Carvano et al. 2010) were converted into the *VRI* system using the same procedure as for the ACAM measurements.

Our colours for the Main Belt asteroids (289) Nenetta and (3819) Robinson are included as well. Both these asteroids have been mineralogically classified as olivine-dominated [defined as S(I) type in the Gaffey et al. 1993 classification] based on their 0.5–2.5 μm spectra (Sanchez et al. 2014). Based on visible (0.44–0.92 μm) spectra alone, Bus & Binzel (2002) classified (289) Nenetta as an A-type asteroid and (3819) Robinson as an S_r-type asteroid. Interestingly, Eureka was also classified as S_r in their work. Our $(V - R)$ colour of (3819) Robinson is lower than that of (289) Nenetta, consistent with the somewhat shallower slope shortward of the reflectance peak for that spectral class as compared to the A type.

Downloaded from https://academic.oup.com/mnras/article-abstract/466/1/489/2608775 by INAF Torino (Osservatorio Astrofisico di Torino) user on 14 July 2020

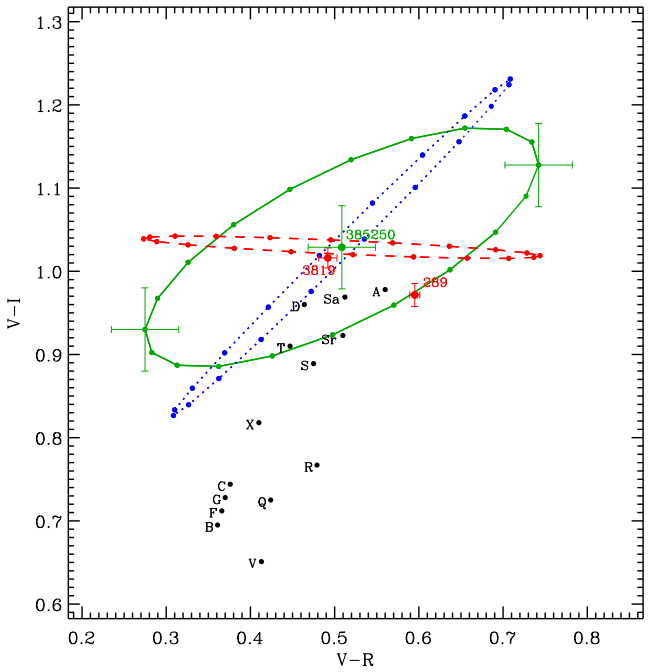

Figure 6. $(V - R)/(V - I)$ colour diagram of the Eureka family member (385250) 2001 DH47 as well as A-class asteroids (289) Nenetta and (3819) Robinson versus mean colours of the different taxonomic classes discussed in the text. The three ellipses shown in the plot represent the systematic uncertainty in the colours of (385250) 2001 DH47 due to the light-curve effect. These are shown for the rotation period solution ($P = 4$ h; green line), as well as for two extreme cases: $P = 3.2$ h (blue dotted line) and $P = 4.8$ h (red dashed line). If our measurements were free from the random error, our estimated colours for this asteroid should be located on one of the eclipses. Note that the random uncertainties (shown by error bars) are smaller than this systematic effect.

We therefore conclude that the colour of (385250) 2001 DH47, after taking into account rotation-related photometric effects, is consistent with the spectroscopic determination of its taxonomy. Taking into account the asteroids' rotational brightness changes will be important in our future attempts to constrain the taxonomic class through colour photometry.

5 DISCUSSION AND CONCLUSIONS

Our spectroscopic and spectrophotometric data confirm that three members of the Eureka family in the L5 Mars Trojan cloud – including the previously observed Eureka – exhibit properties that are best interpreted in terms of a high surface abundance of olivine. Objects sharing the same property, taxonomically classified as members of the A and S_a classes in the DeMeo et al. (2009b) taxonomy, are quite unusual among the asteroid population. As mentioned in the Introduction, there are reasons to believe that olivine-rich bodies were common among planetesimals accreted in the inner regions of the Solar system during the early phases of planetary formation. The current underabundance of such objects may well indicate that most of those that were originally present have been lost – the so-called 'missing mantle problem' (DeMeo et al. 2015). If this interpretation is correct, then it is interesting that we find a small group of these bodies in one of the Mars Trojan clouds. Due to the particular dynamical environment that ensures orbital stability over long time-scales, the Martian Trojan clouds are one of the few places where one would expect to find samples of the first generation of planetesimals accreted in this region. In other words, these asteroids might well be samples of the original building blocks that came together to form Mars and of the other terrestrial planets. The common fate of these bodies elsewhere seems to have been a nearly complete removal, possibly the result of intense collisional evolution (Burbine et al. 1996; Chapman 1997; Sanchez et al. 2014). It is also possible that the dynamical excitation of planetesimals in the current main belt during an early phase of migration of the giant planets (Walsh et al. 2011, 2012) is implicated in the disappearance of these objects.

The fact that these olivine-rich asteroids belong to a group (the Eureka family) of objects that may share a common origin is also interesting. Recent numerical modelling of the family's evolution under planetary gravitational perturbations and the Yarkovsky effect led Ćuk et al. (2015) to conclude that the group is likely a genetic family formed roughly in the last Gyr of the Solar system's history. Whether or not the family sprung off a common parent – a proto-Eureka – has an obvious bearing on the relative abundance of olivine-rich material near Mars in the early Solar system. It is also important to view this in the context of the apparent compositional diversity of the Martian Trojan population overall. Rivkin et al. (2003) obtained visible spectra of Eureka, (101429) 1998 VF31 at L5 and (121514) 1999 UJ7 at L4, later complemented by NIR spectral coverage for the first two asteroids (Rivkin et al. 2007). They found that the latter two asteroids do not share Eureka's taxonomy and concluded that all these objects were once parts of larger bodies that formed separately in different locations of the Solar system.

Future investigations of objects in Mars Trojan clouds should include high-S/N spectra in the visual and NIR spectral regions to help us better understand the compositional relationships. Extending the Mars Trojan inventory down to smaller sizes and determining their rotational characteristics would also help evaluate the stability of these objects in the size regime where non-gravitational perturbations such as the Yarkovsky effect become important.

ACKNOWLEDGEMENTS

This work was supported via a grant (ST/M000834/1) from the UK Science and Technology Facilities Council. Based on observations collected at the European Organisation for Astronomical Research in the Southern Hemisphere under ESO programme 296.C-5030 (PI: A. Christou). We gratefully acknowledge observing grant support from the Institute of Astronomy and Rozhen National Astronomical Observatory, Bulgarian Academy of Sciences. We thank Colin Snodgrass for kindly agreeing to observe asteroid 3819 with ACAM@WHT during program ITP6 and Maxime Devogele for his suggestion to compare our asteroid spectra with laboratory olivine spectra. Astronomical research at the Armagh Observatory and Planetarium is grant-aided by the Northern Ireland Department for Communities (DfC). This research utilizes spectra acquired from the NASA RELAB facility at Brown University. Eureka spectral data utilized in this publication were obtained and made available by The MIT-UH-IRTF Joint Campaign for NEO Reconnaissance. The IRTF is operated by the University of Hawaii under Cooperative Agreement no. NCC 5-538 with the National Aeronautics and Space Administration, Office of Space Science, Planetary Astronomy Program. The MIT component of this work is supported by NASA grant 09-NEOO009-0001, and by the National Science Foundation under Grants Nos. 0506716 and 0907766.

Downloaded from https://academic.oup.com/mnras/article-abstract/466/1/489/2608775 by INAF Torino (Osservatorio Astrofisico di Torino) user on 14 July 2020

REFERENCES

Borisov G., Christou A., Unda-Sanzana E., 2016, Minor Planet Bull., 43, 216

Burbine T. H., Meibom A., Binzel R. P., 1996, Meteorit. Planet. Sci., 31, 607

Bus S. J., Binzel R. P., 2002, Icarus, 158, 146

Carvano J. M., Hasselmann P. H., Lazzaro D., Mothé-Diniz T., 2010, A&A, 510, A43

Chapman C. R., 1997, Nature, 385, 293

Christou A. A., 2013, Icarus, 224, 144

Dandy C. L., Fitzsimmons A., Collander-Brown S. J., 2003, Icarus, 163, 363

de la Fuente Marcos C., de la Fuente Marcos R., 2013, MNRAS, 432, 31

DeMeo F., Binzel R. P., Slivan S. M., Bus S. J., 2009a, NASA Planet. Data Syst., 114

DeMeo F. E., Binzel R. P., Slivan S. M., Bus S. J., 2009b, Icarus, 202, 160

DeMeo F. E., Alexander C. M. O., Walsh K. J., Chapman C. R., Binzel R. P., 2015, in Michel P., DeMeo F. E., Bottke W. F., eds, Asteroids IV. Univ. Arizona Press, Tucson, p. 13

Gaffey M. J., Burbine T. H., Piatek J. L., Reed K. L., Chaky D. A., Bell J. F., Brown R. H., 1993, Icarus, 106, 573

Gourgeot F., Barucci M. A., Alvarez-Candal A., Merlin F., Perna D., Lazzaro D., 2015, A&A, 582, A13

Gutiérrez P. J., Davidsson B. J. R., Ortiz J. L., Rodrigo R., Vidal-Nuñez M. J., 2006, A&A, 454, 367

Jockers K. et al., 2000, Kinematika Fiz. Nebesnykh Tel, 3, 13

Jordi K., Grebel E. K., Ammon K., 2006, A&A, 460, 339

Lim L. F., Emery J. P., Mueller M., Rivkin A. S., Trilling D., Burt B. J., 2011, p. 1199

Moehler S. et al., 2014, A&A, 568, A9

Neese C., 2010, NASA Planet. Data Syst., 123

Rayner J. T., Toomey D. W., Onaka P. M., Denault A. J., Stahlberger W. E., Vacca W. D., Cushing M. C., Wang S., 2003, PASP, 115, 362

Rivkin A. S., Binzel R. P., Howell E. S., Bus S. J., Grier J. A., 2003, Icarus, 165, 349

Rivkin A. S., Trilling D. E., Thomas C. A., DeMeo F., Spahr T. B., Binzel R. P., 2007, Icarus, 192, 434

Sanchez J. A. et al., 2014, Icarus, 228, 288

Scholl H., Marzari F., Tricarico P., 2005, Icarus, 175, 397

Stetson P. B., 1990, PASP, 102, 932

Tholen D. J., 1984, PhD thesis, Univ. Arizona, Tucson

Vernet J. et al., 2011, A&A, 536, A105

Walsh K. J., Morbidelli A., Raymond S. N., O'Brien D. P., Mandell A. M., 2011, Nature, 475, 206

Walsh K. J., Morbidelli A., Raymond S. N., O'Brien D. P., Mandell A. M., 2012, Meteorit. Planet. Sci., 47, 1941

Ćuk M., Christou A. A., Hamilton D. P., 2015, Icarus, 252, 339

This paper has been typeset from a TEX/LATEX file prepared by the author.

Downloaded from https://academic.oup.com/mnras/article-abstract/466/1/489/2608775 by INAF Torino (Osservatorio Astrofisico di Torino) user on 14 July 2020